A Sobolev Norm Based Distance Measure for HARDI Clustering

A Feasibility Study on Phantom and Real Data

Ellen Brunenberg[1], Remco Duits[2,1],
Bart ter Haar Romeny[1], and Bram Platel[3]

[1] Biomedical Engineering, Eindhoven University of Technology
[2] Mathematics and Computer Science, Eindhoven University of Technology
[3] Biomedical Engineering, Maastricht University Medical Center
e.j.l.brunenberg@tue.nl

Abstract. Dissimilarity measures for DTI clustering are abundant. However, for HARDI, the $\mathbb{L}_2$ norm has up to now been one of only few practically feasible measures. In this paper we propose a new measure, that not only compares the amplitude of diffusion profiles, but also rewards coincidence of the extrema. We tested this on phantom and real brain data. In both cases, our measure significantly outperformed the $\mathbb{L}_2$ norm.

1 Introduction

Segmentation of gray matter nuclei in the brain can provide solutions for a multitude of clinical questions. A rich variety of clustering algorithms has been employed for this purpose, together with a large number of dissimilarity measures, mainly focusing on DTI. Wiegell et al. [1] clustered DTI in the thalamus, using k-means and the Frobenius norm. Ziyan et al. used graph cuts [2] on the same data to investigate the angular difference and K-L divergence.

For HARDI, the $\mathbb{L}_2$ norm has been used most often to compare ODFs, possibly represented by spherical harmonic (SH) coefficients. Grassi et al. [3] performed k-medoids clustering in the thalamus using the $\mathbb{L}_2$ norm on the ODFs. Similarly, Descoteaux [4] used the $\mathbb{L}_2$ norm on SH coefficients. Apart from clustering using SH coefficients, there are other ways to represent the ODF. Some studies have implemented mixture models like von Mises-Fisher distributions [5], while others have used a model-free representation of the ODF [6].

In this paper, we propose a new dissimilarity measure for ODFs represented by SH coefficients. Whereas the $\mathbb{L}_2$ norm only compares amplitudes of the diffusion profiles, our Sobolev norm also takes into account whether the extrema coincide.

2 Dissimilarity Measure Based on Sobolev Norm

Consider HARDI-image $U : \mathbb{R}^3 \times S^2 \to \mathbb{R}^+$ and assume it is square integrable, i.e. $U \in \mathbb{L}_2(\mathbb{R}^3 \times S^2)$. By restricting this HARDI-image to two fixed points, say $\mathbf{x}_1, \mathbf{x}_2$ in $\mathbb{R}^3$ we obtain two functions on the 2-sphere

$$S^2 \ni \mathbf{n} \mapsto U(\mathbf{x}_1, \mathbf{n}) \in \mathbb{R}^+ \text{ and } S^2 \ni \mathbf{n} \mapsto U(\mathbf{x}_2, \mathbf{n}) \in \mathbb{R}^+,$$

T. Jiang et al. (Eds.): MICCAI 2010, Part I, LNCS 6361, pp. 175–182, 2010.

which we from now on denote by $U(\mathbf{x}_1, \cdot)$ and $U(\mathbf{x}_2, \cdot)$. These functions can be represented by a so-called glyph $\mathcal{S}_\mu(U)(\mathbf{x}_1)$ and $\mathcal{S}_\mu(U)(\mathbf{x}_2)$ as defined below.

Definition 1. *A glyph of a distribution $U : \mathbb{R}^3 \times S^2 \to \mathbb{R}^+$ on positions and orientations is a surface $\mathcal{S}_\mu(U)(\boldsymbol{x}) = \{\boldsymbol{x} + \mu\, U(\boldsymbol{x}, \boldsymbol{n})\ \boldsymbol{n} \mid \boldsymbol{n} \in S^2\} \subset \mathbb{R}^3$ for some $\boldsymbol{x} \in \mathbb{R}^3$, $\mu > 0$. A glyph visualization of distribution $U : \mathbb{R}^3 \times S^2 \to \mathbb{R}^+$ is a visualization of a field $\boldsymbol{x} \mapsto \mathcal{S}_\mu(U)(\boldsymbol{x})$ of glyphs, with $\mu > 0$ a suitable constant.*

A common approach to compare two glyphs $\mathcal{S}_\mu(U)(\mathbf{x}_1)$ and $\mathcal{S}_\mu(U)(\mathbf{x}_2)$ is to compute the $\mathbb{L}_2$ distance between $U(\mathbf{x}_1, \cdot) : S^2 \to \mathbb{R}^+$ and $U(\mathbf{x}_2, \cdot) : S^2 \to \mathbb{R}^+$:

$$d(U(\mathbf{x}_1, \cdot), U(\mathbf{x}_2, \cdot)) = \sqrt{\int_{S^2} |U(\mathbf{x}_1, \mathbf{n}) - U(\mathbf{x}_2, \mathbf{n})|^2 \, \mathrm{d}\sigma(\mathbf{n})},$$

where σ denotes the usual surface measure on S^2. However, this distance only compares glyph amplitudes. It does not take into account robust regularization and more importantly, it does not consider whether the extrema of the glyphs coincide. Therefore we include a blob-detector [7] in our distance. We do not use higher-order derivatives because they hinder damping before the Nyquist frequency and are more ill-posed due to a higher operator norm.

We have defined the (squared) Sobolev distance between two glyphs as

$$\begin{aligned}
&(\, d_{\alpha,\gamma,t}(\, U(\mathbf{x}_1, \cdot), U(\mathbf{x}_2, \cdot)\,)\,)^2 \\
&:= \int_{S^2} \left| (e^{-t|\Delta_{S^2}|^\alpha} U)(\mathbf{x}_1, \mathbf{n}) - (e^{-t|\Delta_{S^2}|^\alpha} U)(\mathbf{x}_2, \mathbf{n}) \right|^2 \mathrm{d}\sigma(\mathbf{n}) \\
&+ \gamma^{2\alpha} \int_{S^2} \left| |\Delta_{S^2}|^\alpha (e^{-t|\Delta_{S^2}|^\alpha} U)(\mathbf{x}_1, \mathbf{n}) - |\Delta_{S^2}|^\alpha (e^{-t|\Delta_{S^2}|^\alpha} U)(\mathbf{x}_2, \mathbf{n}) \right|^2 \mathrm{d}\sigma(\mathbf{n}) \\
&=: \|U(\mathbf{x}_1, \cdot) - U(\mathbf{x}_2, \cdot)\|^2_{\mathbb{H}^{2\alpha}_t(S^2)}.
\end{aligned} \tag{1}$$

This Sobolev distance basically is a sum of a standard (smoothed) $\mathbb{L}_2$ part (first integral) and a (smoothed) blob-sensitive second part (second integral). Next we provide a brief explanation on the involved parameters:

- The parameter $\alpha \in [\frac{1}{2}, 1]$ denotes the α-scale space regularization on a sphere [8], applied at time $t \geq 0$ (or scale $t^{\frac{1}{2\alpha}}$). Note that $e^{-t|\Delta_{S^2}|^\alpha}$ denotes a smoothing operator generated by a fractional power of the Laplace-Beltrami operator Δ_{S^2}, i.e. $W_U(\mathbf{x}, \mathbf{n}, t) = e^{-t|\Delta_{S^2}|^\alpha} U(\mathbf{x}, \mathbf{n})$ is the solution of

$$\begin{cases} \frac{\partial W_U}{\partial t}(\mathbf{x}, \mathbf{n}, t) = -|\Delta_{S^2}|^\alpha W_U(\mathbf{x}, \mathbf{n}, t), & \mathbf{x} \in \mathbb{R}^3, \mathbf{n} \in S^2, t \geq 0, \\ W_U(\mathbf{x}, \mathbf{n}, 0) \ = U(\mathbf{x}, \mathbf{n})\ . \end{cases} \tag{2}$$

- The parameter $t \geq 0$ determines the stopping time of the spherical α-scale space regularization.
- The parameter γ (physical dimension $[\mathrm{Length}]^2$) determines the influence of the blob-sensitive and the intensity-sensitive $\mathbb{L}_2$ part of the Sobolev norm.

The blob-sensitive part is the same as the total difference of all scale space dynamics of the glyphs. This follows from the fact that (1) can be rewritten as

$$\int_{S^2} |W(\mathbf{x}_1,\mathbf{n},t) - W(\mathbf{x}_2,\mathbf{n},t)|^2 + \gamma^{2\alpha} \left|\tfrac{dW}{dt}(\mathbf{x}_1,\mathbf{n},t) - \tfrac{dW}{dt}(\mathbf{x}_2,\mathbf{n},t)\right|^2 \mathrm{d}\sigma(\mathbf{n})$$
$$= \int_{S^2} |W(\mathbf{x}_1,\mathbf{n},t) - W(\mathbf{x}_2,\mathbf{n},t)|^2 + \gamma^{2\alpha} \left||\Delta_{S^2}|^{\alpha} W(\mathbf{x}_1,\mathbf{n},t) - |\Delta_{S^2}|^{\alpha} W(\mathbf{x}_2,\mathbf{n},t)\right|^2 \mathrm{d}\sigma(\mathbf{n}),$$

where we use $W = W_U$. Roughly speaking, $\gamma > 0$ balances the similarity of the extrema and the similarity of the amplitudes of $\mathcal{S}_\mu(U)(\mathbf{x}_1)$ and $\mathcal{S}_\mu(U)(\mathbf{x}_2)$.

Recall that the spherical harmonics $\{Y_{lm}\}_{l=0,\ldots,\infty}^{m=-l,\ldots,l}$ form an orthonormal basis of $\mathbb{L}_2(S^2)$, i.e.

$$(Y_{lm}, Y_{l'm'})_{\mathbb{L}_2(S^2)} := \int_{S^2} \overline{Y_{lm}(\mathbf{n})}\, Y_{l'm'}(\mathbf{n})\, \mathrm{d}\sigma(\mathbf{n}) = \delta_{ll'}\delta_{mm'}$$
$$\text{and } \forall_{l=0,\ldots,\infty} \forall_{m=-l\ldots,l} \; : \; (f, Y_{lm})_{\mathbb{L}_2(S^2)} = 0 \Rightarrow f = 0.$$

with Y_{lm} eigenvalues of the negative semi-definite, fractional Laplacian operator

$$-|\Delta_{S^2}|^{\alpha} Y_{lm} = -l^{\alpha}(l+1)^{\alpha} Y_{lm}$$

and thereby the solution of (2) is given by

$$\begin{aligned} W(\mathbf{x},\mathbf{n}(\theta,\phi),t) &= \sum_{l=0}^{\infty} \sum_{m=-l}^{l} (Y_{lm}, U(\mathbf{x},\cdot))_{\mathbb{L}_2(S^2)}\, e^{-t|\Delta_{S^2}|^{\alpha}} Y_{lm}(\theta,\phi) \\ &= \sum_{l=0}^{\infty} \sum_{m=-l}^{l} (Y_{lm}, U(\mathbf{x},\cdot))_{\mathbb{L}_2(S^2)}\, e^{-t(l(l+1))^{\alpha}} Y_{lm}(\theta,\phi). \end{aligned} \tag{3}$$

In particular for $\alpha = \frac{1}{2}$ (Poisson scale space [8,9]) the solution of (2) is nearly equivalent to outward harmonic extension of the initial distribution $\mathbf{n} \mapsto U(\mathbf{n})$ on the 2-sphere, where one must set the radius $\rho = e^{-t}$, since

$$\rho\ \mathbf{n}(\theta,\phi) = (\rho\cos\phi\sin\theta, \rho\sin\phi\sin\theta, \rho\cos\theta) \mapsto \rho^l Y_{lm}(\theta,\phi)$$

is a harmonic function on $\mathbb{R}^3$ and $\rho^l = e^{-tl} \approx e^{-t\sqrt{(l+1)l}}$ for l sufficiently large. So intuitively one may consider a radial scale axis for scale spaces on glyphs. If we expand $U(\mathbf{x}_1,\cdot)$ and $U(\mathbf{x}_2,\cdot)$ into the orthonormal basis of spherical harmonics:

$$U(\mathbf{x}_i,\mathbf{n}(\theta,\phi)) = \sum_{l=0}^{\infty} \sum_{m=-l}^{l} c_i^{lm}\, Y_{lm}(\mathbf{n}(\theta,\phi))\ , i = 1,2,$$
$$\text{with } Y_l^m(\phi,\theta) = \sqrt{\tfrac{(2l+1)(l-|m|)!}{4\pi(l+|m|)!}} P_l^m(\cos\theta) e^{im\phi},$$

with P_l^m the associated Legendre polynomial of degree l and order m, and with $c_i^{lm} = (Y_{lm}, U(\mathbf{x}_i,\cdot))_{\mathbb{L}_2(S^2)}$, $i = 1,2$, the squared Sobolev distance (1) reads

$$(\, d_{\alpha,\gamma,t}(\, U(\mathbf{x}_1,\cdot), U(\mathbf{x}_2,\cdot)\,)\,)^2 = \sum_{l=0}^{\infty} \sum_{m=-l}^{l} |c_1^{lm} - c_2^{lm}|^2\, \tilde{m}_l^{\alpha,\gamma,t}.$$

This is a weighted ℓ_2 inner product on the coefficients, so we only have to study the multiplier

$$\tilde{m}_l^{\alpha,\gamma,t} = (1 + (\gamma\, l(l+1))^{2\alpha})\, e^{-2t(l(l+1))^{\alpha}}$$

to see how the different spherical harmonics are weighted in the Sobolev distance. Note that if $\gamma = t = 0$, the Sobolev norm is equivalent to the $\mathbb{L}_2$ norm.

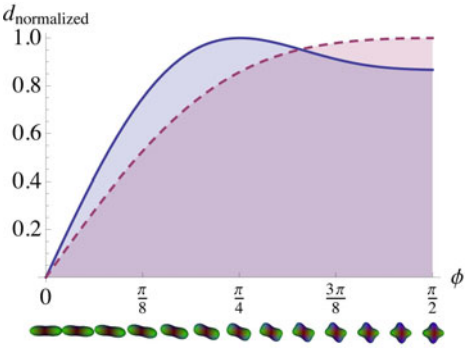

Fig. 1. Behavior of the Sobolev (blue, solid line) and the $\mathbb{L}_2$ norm (red, dashed line) for a combination of two single fiber profiles generated with angle ϕ in between

Analytical Example. To qualify the Sobolev and $\mathbb{L}_2$ norm, we investigated several diffusion profiles. The basis for each profile is a single fiber distribution

$$U(\mathbf{n}) = (\mathbf{n}^T M \mathbf{n})^4,$$

with M the diagonal diffusion matrix with $\{1, \epsilon, \epsilon\}$ as elements and $\mathbf{n} \in S^2$ describing the tesselation orientations. The fourth power is taken to sharpen the result. To this static part, a second single fiber profile is added, that is rotated over angle ϕ with respect to the first profile. The total profile then amounts to

$$U(\mathbf{n}) = (\mathbf{n}^T M \mathbf{n})^4 + (\mathbf{n}^T R_\phi M R_\phi^T \mathbf{n})^4,$$

with R_ϕ a transformation matrix resulting in a clockwise rotation over angle ϕ. We compare default diffusion profile f ($\phi = 0, f = U(\mathbf{x}_1, \cdot)$) with a set of profiles g with ϕ varying between 0 and $\pi/2$ ($g = U(\mathbf{x}_2, \cdot)$). Figure 1 shows the results for both the Sobolev and $\mathbb{L}_2$ norm, normalized by their maximum response:

$$d_{\text{normalized}}(f, g) = \frac{\|f - g\|}{\max\limits_g \|f - g\|}.$$

It can be seen that for $\phi = \pi/4$, the diffusion profile has maxima that do not overlap with those at $\phi = 0$, while two of the four maxima at $\phi = \pi/2$ do coincide. The Sobolev norm clearly punishes the deviations in extrema. For small differences in angle ϕ, the Sobolev norm gives a larger response, but in the case of partly overlapping extrema, towards $\phi = \pi/2$, the Sobolev norm is again lower than its $\mathbb{L}_2$ counterpart. The latter yields its maximum at $\phi = \pi/2$, because the amplitudes of the diffusion profiles differ most at that point.

Implementation. In practice, discretization of the continuous spherical harmonics is done by the pseudo-inverse of the inverse spherical harmonic transform (DISHT) [10]. Similar to Descoteaux [4], we use only even orders of spherical harmonics to represent our HARDI data, i.e. order $l = 0, 2, 4, \ldots, L_{max}$. As m still has range $-l, \ldots, 0, \ldots, l$, the total number of SH coefficients is defined as

$n_{SH} = \frac{1}{2}(L_{max}+1)(L_{max}+2)$. We define a single index j in terms of l and m such that $j(l,m) = (l^2+l+2)/2+m$ and compute the spherical harmonic coefficients $\mathbf{s} \in \mathbb{C}^{n_{SH}}$ from the values $\mathbf{f} \in (\mathbb{R}^+)^{N_o}$ by means of

$$\mathbf{s} = (DISHT)^+[\mathbf{f}] = (\overline{\mathbf{M}}\mathbf{M}^T)^{-1}\overline{\mathbf{M}}\mathbf{f}\,,$$

with $\mathbf{M} = [M_k^j] = [\frac{1}{\sqrt{C}} Y_{m(j)}^{l(j)}(\mathbf{n}_k)]$ and $C = \sum_{j=1}^{n_{SH}} |Y_{m(j)}^{l(j)}(0,0)|^2$, such that $\mathbf{M}^\dagger\mathbf{M}$ has a diagonal of ones. If $\mathbf{f}_i \in (\mathbb{R}^+)^{N_o}$ denotes the discrete data on $U(\mathbf{x}_i,\cdot)$, $i=1,2$, i.e. $(\mathbf{f}_i)_k = U(\mathbf{x}_i,\mathbf{n}_k)$, $k=1,\ldots,N_o$ then the discrete Sobolev norm is

$$d^{\text{discrete}}_{\alpha,\gamma,t}(\mathbf{f}_1,\mathbf{f}_2) = \sqrt{\sum_{j=1}^{n_{SH}} |(DISHT)^+[\mathbf{f}_2][j] - (DISHT)^+[\mathbf{f}_1][j]|^2 \; \tilde{m}_{l[j]}^{\alpha,\gamma,t}}\,.$$

3 Phantom and Real Brain Data

We computer generated a HARDI phantom, employing a multitensor model [11], with 121 different gradient directions and b-value 3000 s/mm^2. The phantom consists of 18 columns with different diffusion profiles, namely single fibers at angles $\{0,1,3,6,10,15,21,28,36,45\}$ degrees, two fibers crossing in-plane at angles $\{40,45,55,70,90\}$ degrees, and three fibers crossing in-plane at angles $\{30,40,60\}$ degrees. Each column contains the original profile, followed by ten times this profile with Rician noise added, by applying the transformation

$$(\ (\mathbf{y},\mathbf{n}) \mapsto U(\mathbf{y},\mathbf{n})\ ) \mapsto (\ (\mathbf{y},\mathbf{n}) \mapsto \sqrt{(U(\mathbf{y},\mathbf{n})\cos\eta_1+\eta_2)^2 + (U(\mathbf{y},\mathbf{n})\sin\eta_1+\eta_3)^2}\ )\,,$$

where $\eta_2,\eta_3 \sim \mathcal{N}(0,\sigma)$ normally distributed and η_1 uniformly distributed over $[0,2\pi)$. To obtain data with a realistic SNR of 30, σ was chosen to be 0.1. Using the Funk-Radon transform [4], the simulated signal was converted to spherical harmonic coefficients, with $L_{max} = 12$. Comparing the ℓ_2 norm of the SH coefficients, the noise was shown to lead to a disturbance of approximately 10%.

We also tested our algorithm on real data, analogous to for example Grassi et al. [3]. Human brain diffusion MRI data were acquired at 3T, measuring 52 slices of 128x128 2-mm isotropic voxels, using TE 85 ms, 128 unique gradient directions and b-value 2000 s/mm^2. The data were registered onto the MNI152 template and the accompanying Talairach atlas, using an affine transformation within FSL [12]. Subsequently, an ROI of 30 pixels wide and 39 pixels high, containing the subject's right thalamus, was selected on an axial slice. The data were again transformed to spherical harmonic coefficients ($L_{max} = 12$).

4 Parameter Tuning

The Sobolev norm contains three parameters – α, γ, t – that needed tuning, in order to yield the desired behavior. Equivalent to Lindeberg [7], α was set to 1, the value for Gaussian regularization. We chose t to be 0, as our data were sufficiently smooth. In addition, the $\mathbb{L}_2$ norm lacks regularization, so setting $t = 0$ enables a fair comparison. To assess the optimal value for γ, we performed

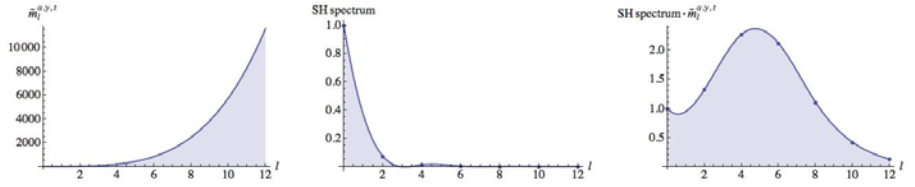

Fig. 2. Left: Behavior of the Sobolev multiplier $\tilde{m}_l^{\alpha,\gamma,t}$ for $\{\alpha = 1, \gamma = 0.69, t = 0\}$ and l from 0 to 12. **Middle:** Normalized mean spectrum of spherical harmonic coefficients of the phantom diffusion profiles. **Right:** Product of multiplier and spectrum.

a 1-nearest-neighbor classification, using the 18 original profiles of the phantom (i.e. without noise) as training and the whole phantom as test set, while γ was varied from 0 to 0.8 in steps of 0.01. The performance of the $\mathbb{L}_2$ norm for this phantom is 71.2%. However, using the Sobolev norm with $\gamma \geq 0.69$, the phantom classification reached a performance of 100%.

The behavior of the multiplier $\tilde{m}_l^{\alpha,\gamma,t}$ for $\{\alpha = 1, \gamma = 0.69, t = 0\}$ is plotted in Fig. 2 (left). It can be seen that the function exponentially rises towards higher values of l. However, the spherical harmonic coefficients of the used diffusion profiles at higher orders are quite small, as can be seen in Fig. 2 (middle). This means that the product of the multiplier and the spectrum is damped well enough to be truncated at $l = 12$ and avoid Gibbs artifacts (see Fig. 2 (right)).

5 K-Means Clustering

Following the example set by Wiegell et al. [1], we performed k-means clustering. For both the synthetic phantom and the real brain data, a set of seed points to serve as initial centroids was determined manually. The seed point placement for the phantom was straightforward, with a seed point in the middle of each column. The real brain ROI was masked using the atlas' thalamus segmentation, while

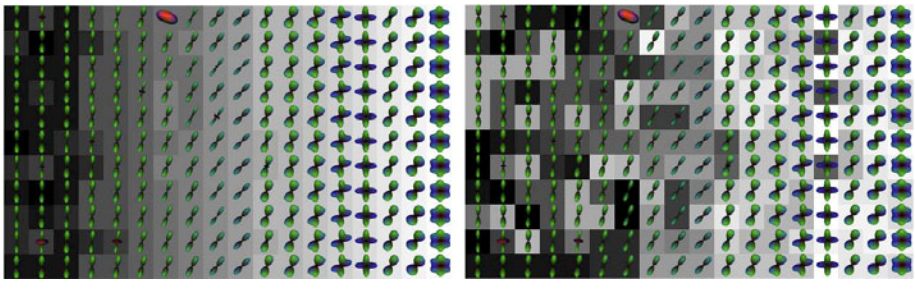

Fig. 3. Left: Result of $\mathbb{L}_2$ norm (20.7% correctly classified). **Right:** Result of Sobolev norm with $\{\alpha = 1, \gamma = 0.69, t = 0\}$ (73.7 % correctly classified). The diffusion profiles are visualized as min-max normalized Q-ball glyphs using SH coefficients up to $l = 8$.

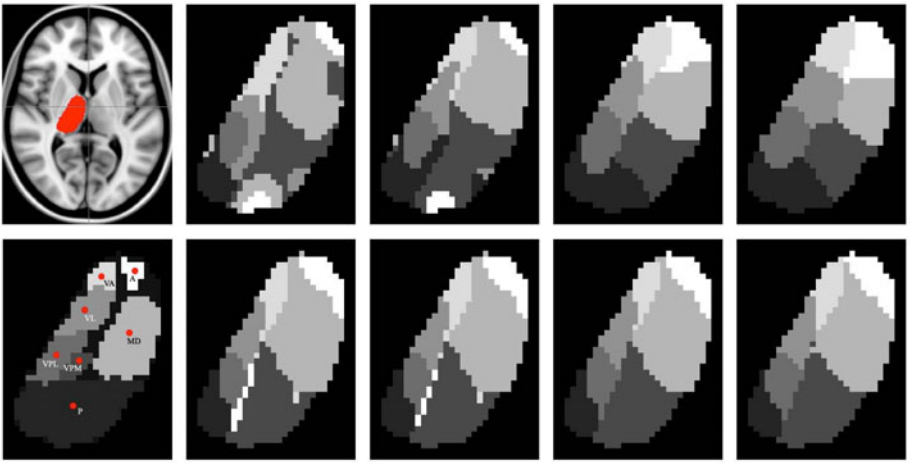

Fig. 4. Leftmost column: Thalamus ROI (top) and nuclei atlas labels (bottom). **Other columns:** Results using $\mathbb{L}_2$ (top) and Sobolev norm (bottom, $\{\alpha = 1, \gamma = 0.69, t = 0\}$). The ratio between diffusion and spatial information was varied, from left to right: ratio 1:1; $\frac{1}{5}$·weight factor (as defined in [1]); 1·weight factor; 5·weight factor.

the seven seed points for this ROI were chosen to lie in the different nuclei of the thalamus, as defined by the atlas (see Fig. 4 (bottom left)). To associate each point of the data sets with a cluster, we used both the $\mathbb{L}_2$ norm and the Sobolev norm with the parameters calculated in Section 4: $\{\alpha = 1, \gamma = 0.69, t = 0\}$. The new centroids of each cluster were calculated as the mean of the voxel positions of all connected points. However, as our dissimilarity measures only concerned diffusion information, we calculated the distance between each data point and the mean diffusion profile of all points associated with each cluster.

The results of the k-means clustering for the phantom can be seen in Fig. 3. The $\mathbb{L}_2$ norm yields only a 20.7% correct classification (left). Clearly, the Sobolev norm has performed much better, obtaining 73.7% correctly classified diffusion profiles, as shown on the right-hand side. With respect to the thalamus ROI, in Fig. 4 we can see that the k-means clustering succeeds to classify the thalamus nuclei reasonably well. The pulvinar and ventral posterior medial nucleus are segmented but cannot be separated. The results of the Sobolev norm seem more stable, i.e. less dependent on the weight factor between diffusion and spatial information, as defined by Wiegell et al. [1], than the results of the $\mathbb{L}_2$ norm.

6 Discussion

In this paper, we introduced a new dissimilarity measure that can be employed for clustering of HARDI data. Instead of comparing only the amplitudes of the diffusion profiles, our Sobolev norm also takes into account whether the extrema of the profiles coincide. We illustrated the behavior of our norm for some simple synthetic glyphs and then built a more difficult phantom. The optimal

parameters for our norm were found using 1-nearest-neighbor clustering of this phantom, and these parameters were used for the subsequent k-means clustering. The Sobolev norm consistently performed better than the $\mathbb{L}_2$ norm, for both the phantom and the real brain data.

In order to improve upon this work, a clustering algorithm that is not biased by the number and placement of seed points could be employed, for example spectral clustering involving graph cuts [13]. It will remain a challenge to interpret the results of the real data, due to the absence of a proper ground truth.

Acknowledgments

Ellen Brunenberg is supported by the Netherlands Organization for Scientific Research (NWO). The authors would like to thank Bart Spronck, Vesna Prčkovska, and Markus van Almsick for their help.

References

1. Wiegell, M.R., Tuch, D.S., Larsson, H.B.W., Wedeen, V.J.: Automatic segmentation of thalamic nuclei from diffusion tensor magnetic resonance imaging. Neuroimage 19(2), 391–401 (2003)
2. Ziyan, U., Tuch, D., Westin, C.F.: Segmentation of thalamic nuclei from DTI using spectral clustering. In: Larsen, R., Nielsen, M., Sporring, J. (eds.) MICCAI 2006. LNCS, vol. 4191, pp. 807–814. Springer, Heidelberg (2006)
3. Grassi, A., Cammoun, L., Pollo, C., Hagmann, P., Meuli, R., Thiran, J.P.: Thalamic nuclei clustering on high angular resolution diffusion images. ISMRM 16, 1777 (2008)
4. Descoteaux, M.: High Angular Resolution Diffusion MRI: from Local Estimation to Segmentation and Tractography. PhD thesis, INRIA Sophia Antipolis (2008)
5. McGraw, T., Vemuri, B., Yezierski, R., Mareci, T.: Segmentation of high angular resolution diffusion MRI modeled as a field of von Mises-Fisher mixtures. In: Leonardis, A., Bischof, H., Pinz, A. (eds.) ECCV 2006. LNCS, vol. 3953, pp. 463–475. Springer, Heidelberg (2006)
6. Goh, A., Lenglet, C., Thompson, P.M., Vidal, R.: A nonparametric Riemannian framework for processing high angular diffusion images (HARDI). In: CVPR, pp. 2496–2503 (2009)
7. Lindeberg, T.: Scale-space behaviour of local extrema and blobs. J. Math. Imaging Vision 1(1), 65–99 (1992)
8. Duits, R., Felsberg, M., Florack, L.: α scale spaces on a bounded domain. In: Scale Space Conference, pp. 494–510 (June 2003)
9. Felsberg, M., Duits, R., Florack, L.: The monogenic scale space on a bounded domain and its applications. Int. J. Comput. Vision 2-3(64), 187–201 (2005)
10. Duits, R., Franken, E.: Left-invariant diffusions on the space of positions and orientations and their application to crossing-preserving smoothing of hardi images. Int. J. Comput. Vision (2010), http://dx.doi.org/10.1007/s11263--010--0332--z
11. Söderman, O., Jönsson, B.: Restricted diffusion in cylindrical geometry. J. Magn. Reson. Series A 117(1), 94–97 (1995)
12. Jenkinson, M., Smith, S.: A global optimisation method for robust affine registration of brain images. Med. Image Anal. 5(2), 143–156 (2001)
13. Brunenberg, E., Pelgrim, E., ter Haar Romeny, B., Platel, B.: k-means and graph cuts clustering of diffusion MRI in rat STN. ISMRM 18, 4045 (2010)